

# *In situ* X-Ray Diffraction Analysis of Carbon Partitioning During Quenching of Low Carbon Steel

JÉRÉMY EPP, THOMAS HIRSCH, and CAROLINE CURFS

*In situ* X-ray diffraction investigations of phase transformations during quenching of low carbon steel were performed at the European Synchrotron Radiation Facility (ESRF, Grenoble, France) at beamline ID11. A dynamic stabilization of the retained austenite during cooling below martensite start was identified, resulting in an amount of retained austenite of approximately 4 vol pct. The reason for this dynamic stabilization is a carbon partitioning occurring directly during quenching from martensite (and a small amount of bainite) into retained austenite. A carbon content above 0.5 mass pct was determined in the retained austenite, while the nominal carbon content of the steel was 0.2 mass pct. The martensitic transformation kinetic was compared with the models of Koistinen-Marburger and a modification proposed by Wildau. The analysis revealed that the Koistinen-Marburger equation does not provide reliable kinetic modeling for the described experiments, while the modification of Wildau well describes the transformation kinetic.

DOI: 10.1007/s11661-012-1087-7

© The Minerals, Metals & Materials Society and ASM International 2012

## I. INTRODUCTION

MARTENSITIC transformation in steels has now been investigated for more than 100 years.<sup>[1–5]</sup> The interest in martensitic transformations is still very high as numerous industrial applications need this transformation to improve wear resistance, mechanical properties, and fatigue properties of parts in daily productions.<sup>[6]</sup> Moreover, new interest in fundamentals of martensitic transformations has appeared in the last decades with the challenges of computer simulation, where kinetics and other phenomenon should be well described to obtain reliable simulation results.<sup>[7–9]</sup>

Some recent investigations on medium carbon and low alloyed steels have focused on the characterization of aging/tempering processes and on autotempering, which means tempering effects occurring directly during quenching or bainitic treatments.<sup>[10–12]</sup> From these studies, it was found that retained austenite is mostly present in the form of thin films (of several nanometers in width) between the martensite laths.<sup>[10,11]</sup> Carbon diffusion occurs from the original martensitic phase either into the surrounding lattice defects (like voids, dislocations, *etc.*) or into the retained austenite even at cooling rates up to  $10^3$  K/s.<sup>[10–12]</sup> Strong carbon enrichment at the interface between retained austenite and martensite is then to be expected and was found.<sup>[11]</sup> Hence, the carbon enrichment of the retained austenite induces a stabilization of retained austenite, which depends on the cooling rate.<sup>[10]</sup>

New heat treatments called “Quenching and Partitioning” using that large potential for carbon to diffuse out of the freshly formed martensite were even developed.<sup>[13,14]</sup> To enrich the retained austenite and not to precipitate carbides, the alloys used for those treatments usually contain a high amount of silicon (typically from 0.6 to 2 wt pct) as silicon retards the precipitation of carbides.<sup>[13]</sup>

As most investigations of carbon partitioning during quenching of steel samples were performed on the final state of heat-treated samples, reliable information about the kinetics and generally about ongoing processes are missing.

*In situ* X-ray diffraction (XRD) analysis has become a powerful method for materials characterization stimulated by constant advances in instrumentation and data processing. This method allows, contrarily to dilatometry or resistivity measurements, for obtaining time-resolved precise quantitative information about every phase present in the investigated material.<sup>[15,16]</sup>

In the present investigation, the method of *in situ* XRD analysis was applied to characterize the behavior of a typical case carburizing steel grade (AISI 5120) during rapid cooling. The kinetics of phase transformation and the evolution of carbon contents in the phases were considered. Moreover, models for the description of transformation kinetics were compared and optimized.

## II. EXPERIMENTAL

### A. Materials

*In situ* X-ray diffraction experiments were performed at the European Synchrotron Radiation Facility (ESRF) in Grenoble, France, on beam line ID11. The experiments were executed with a commercial heating

---

JÉRÉMY EPP, Research Engineer, and THOMAS HIRSCH, Research Director, are with the Stiftung Institut fuer Werkstofftechnik, 28359 Bremen, Germany. Contact e-mail: epp@iwt.bremen.de  
CAROLINE CURFS, Senior Scientist, is with the ESRF, F-38043 Grenoble Cedex, France.

Manuscript submitted November 29, 2010.

Article published online March 17, 2012

device (Instron, Pfungstadt, Germany) allowing a controlled heating of samples ( $1.5 \times 1.5 \times 40$  mm) by resistivity. The chemical composition of the investigated AISI 5210 steel is provided in Table I.

A micrograph of one sample in its initial state is shown in Figure 1.

The microstructure consists of ferrite and pearlite bands at approximately  $25 \mu\text{m}$  in width.

Electron microprobe analysis showed that carbon, manganese, and chromium concentrations present

variations with the period of the microstructure (approximately  $25 \mu\text{m}$ ). Figure 2 shows a mapping of element concentrations in a region of  $100 \times 200 \mu\text{m}$ . An average concentration over the height is plotted as well. On the Mn and Cr mappings, the banded structure can be clearly observed, resulting in local average concentrations between 1.2 and 1.55 mass pct for Mn and 1.0 and 1.25 mass pct for Cr. The carbon concentration presents fluctuations between 0.1 and 0.45 mass pct.

**Table I. Chemical Composition of the Investigated Steel in Mass Pct**

C	Si	Mn	P	S	Cr	Mo	Ni	Cu	Al
0.204	0.23	1.35	0.011	0.020	1.02	0.03	0.1	0.12	0.04

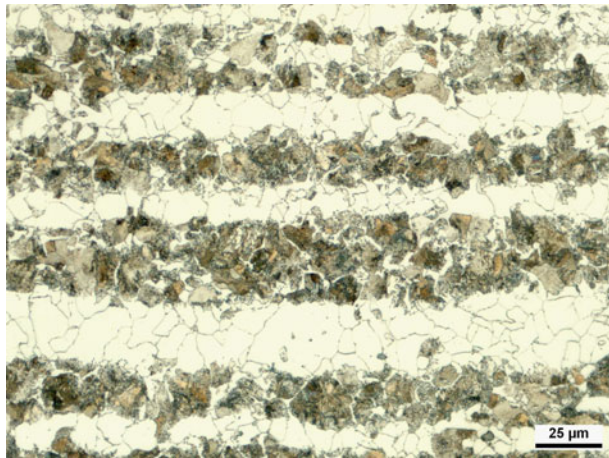


Fig. 1—Microstructure of the investigated steel in its initial state.

### B. In Situ XRD Experiments During Quenching

The following heat treatment cycle was used: a controlled heating with a rate of 10 K/s up to the austenitizing temperature ( $T_A$ ) of 1173 K ( $900^\circ\text{C}$ ) followed by a soaking time of 10 minutes and quenching to room temperature. The huge mass of the clamping tools allowed for quenching of samples without use of any other quenching media. The cooling curve measured on one sample is provided in Figure 3.

Constant argon purging was used to avoid oxidation of the surface. The temperature was controlled by using two thermocouples welded on the surface of the samples. One type R thermocouple was for the temperature control of the heating, while a type K thermocouple was used for more precise temperature measurement in the low-temperature range.

During the entire heat treatment cycle, diffraction frames were recorded in transmission mode with the FRELON (ESRF, Grenoble, France) camera<sup>[17]</sup> using an exposition time of 0.4 seconds for each frame during quenching. The beam energy was 71 keV, and the primary beam size was set at maximum (approximately  $100 \mu\text{m}$  high and  $300 \mu\text{m}$  width). This beam size of ID11 produced the best statistical conditions as possible in terms of diffracting domains.

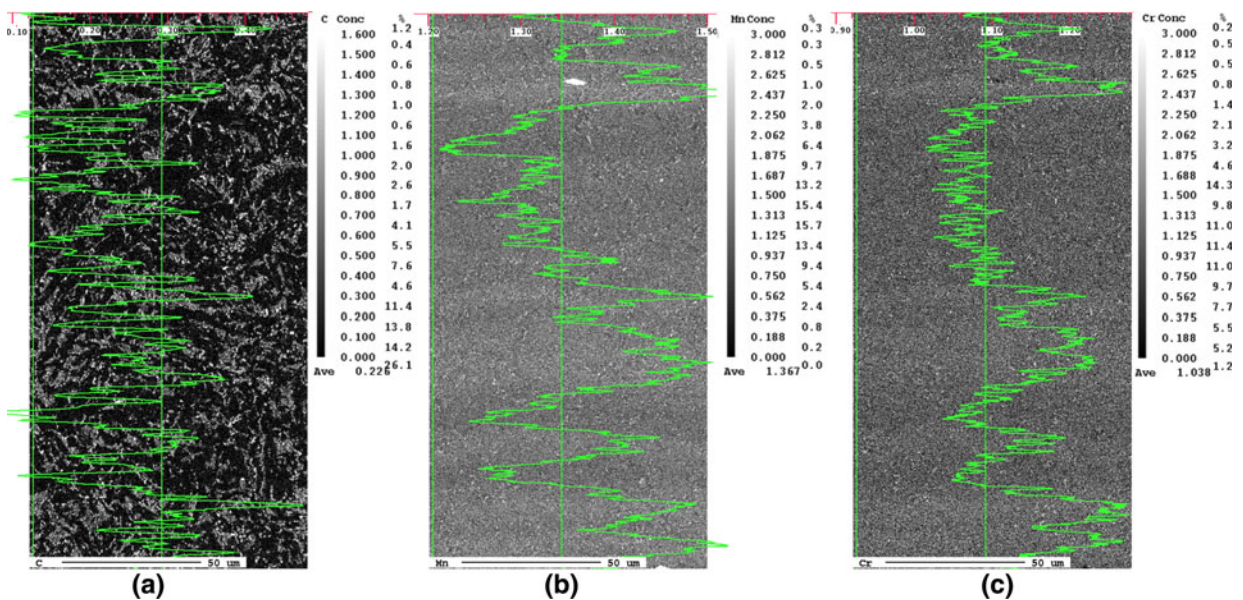


Fig. 2—Electron probe microanalyses of the carbon (a), manganese (b), and chromium (c) concentration in a region of  $100 \times 200 \mu\text{m}$  in a sample before heat treatment.



### C. Analysis of the Recorded Diffraction Frames

To get the information about the instrumental contribution on the diffraction patterns, a standard material ( $\text{LaB}_6$  powder) was measured before. The recorded frames were integrated with the program Fit2d developed at ESRF after background correction for further analysis.<sup>[18]</sup>

The analysis of diffraction patterns after integration has been performed with the Rietveld refinement software TOPAS from Bruker AXS (Karlsruhe, Germany). First, the  $\text{LaB}_6$  measurement was refined to obtain the instrumental function that was then used for all refinements.

X-ray analysis of a fine polycrystalline material will result in a convolution of all microstructural features.<sup>[19]</sup> Different phases are present here, and each phase may contribute in different way to the diffraction pattern according to local textures, anisotropic size and strain broadening, as well as stacking faults. To optimize refined parameters, a pattern recorded after heat treatment was used. The fit of measured data was quite good with the addition of a slight peak scaling. Some strain and size broadening was introduced to model the peak

widths. The model and refinement parameters obtained were then fixed and used for the analysis of the temperature-dependent X-ray diffraction patterns obtained during quenching of the samples.

### III. RESULTS AND DISCUSSION

After *in situ* experiments, one sample was prepared for metallographic investigations. Figure 4 presents the core of the sample (a) and the surface at high magnification (b). The banded structure present before heat treatment (Figure 1) can almost not be identified anymore in Figure 4(a). As shown in Figure 5, the carbon concentration is now very homogeneous so that only slight effects from Mn and Cr segregation are expected on the microstructure. Retained austenite cannot be distinguished even at high magnification. The microstructure at the surface (Figure 4(b)) presents some ferrite in a layer of approximately  $30\ \mu\text{m}$ . This might be from a slight decarburization of the surface.

Electron microprobe analysis was performed after heat treatment to examine the effect of heat treatment on the element distribution. The results of these measurements are presented in Figure 5 for carbon, manganese, and chromium. The scaling of the images is the same as in Figure 2. It can be noticed that the carbon concentration is absolutely homogeneous in the whole examined region. On the contrary, the manganese and chromium distribution still present a banded distribution with concentrations varying between 1.25 and 1.55 mass pct for manganese and 1.05 and 1.25 mass pct for chromium. As expected, the heat treatment did not affect the element distribution of chromium and manganese.

To support the interpretation of results obtained from *in situ* experiments, a comparison with a continuous cooling transformation (CCT) diagram of the considered steel can be done. Figure 6 presents a CCT diagram for 21MnCr5 steel with one measured cooling curve. A small amount of bainite can be expected to form,

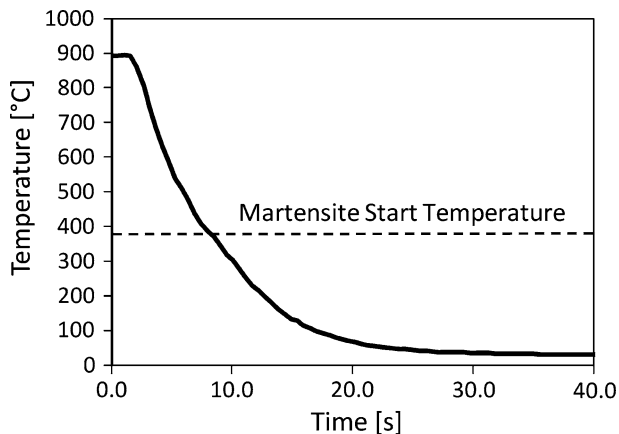


Fig. 3—Cooling curve measured at one investigated sample.

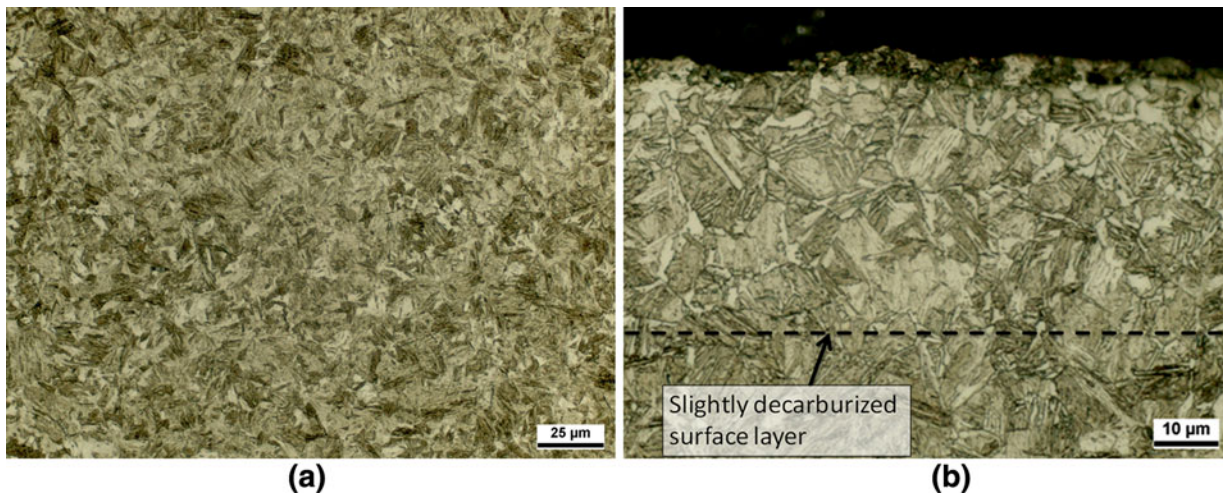


Fig. 4—Microstructure of the core at low magnification (a) and of the surface at high magnification (b) after heat treatment.

starting around 773 K (500 °C). Moreover, as shown in Figure 5, local variations in manganese and chromium are still present after heat treatment. This will induce a slight shift of the bainitic nose to shorter times and higher temperatures for poor regions and to longer times and lower temperatures for enriched regions.<sup>[20]</sup>

The frames recorded during the quenching process of a sample were integrated, and four diffraction patterns collected at important points of the cooling are presented in Figure 7. It can be observed that the data quality is very good with high intensities and sharp diffraction lines. With these data, it was possible to extract reliable information about the transformation kinetics.

With the knowledge of the CCT diagram and the micrographs presented in Figure 4, it is possible to deduce which phases were built during cooling. At the end of austenitizing, the microstructure contains 100 pct of austenite. During cooling, at a temperature of approximately 923 K (650 °C), diffraction lines of a body-centered cubic (BCC) phase appear. According to the CCT diagram, no phase should form at this temperature. However, it is known that slight surface decarburization can occur during *in situ* experiments even with inert gas protection.<sup>[15,16]</sup> This effect combined with possible Mn and Cr fluctuations can lead to the formation of ferrite in surface layers as observed on the micrographs (Figure 4(b)).

From the CCT diagram, a small amount of bainite can be expected to form during cooling, starting at temperatures around 773 K (500 °C). This is indeed observed on the collected XRD patterns. From XRD measurements, martensite with a body centered tetragonal (BCT) structure starts to form around 663 K (390 °C), which is consistent with the  $M_s$  temperature predicted by the CCT diagram. At room temperature after cooling, a small amount of retained austenite is still present (Figure 7).

Rietveld analysis of diffraction patterns from the end of the austenitizing and during cooling to room temperature allowed obtaining the precise evolution of phase fractions. Figure 8 shows the evolution of average phase fractions during cooling obtained from two experiments using the same heat treatment parameters. In the high temperature range (between 923 K (650 °C) and 793 K (520 °C)), the small amount of BCC phase that is probably ferrite remains almost constant around 2 vol pct.

Below 793 K (520 °C), a BCC phase forms with a high rate. As mentioned, the formation of bainite is expected in this temperature range. An amount of 17 vol pct bainite is present at 663 K (390 °C) where the martensitic transformation starts. During the formation of bainite, carbide precipitation normally occurs together with the creation of bainitic ferrite. The appearance of carbide diffraction lines should be observed in the

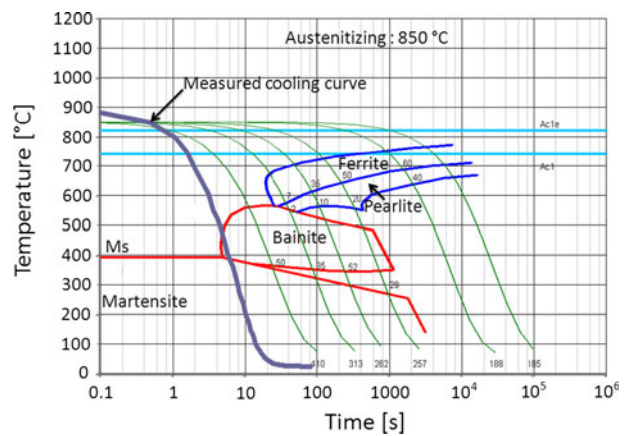


Fig. 6—CCT diagram of 21MnCr5 steel with the cooling curve measured during the experiments.<sup>[21]</sup>

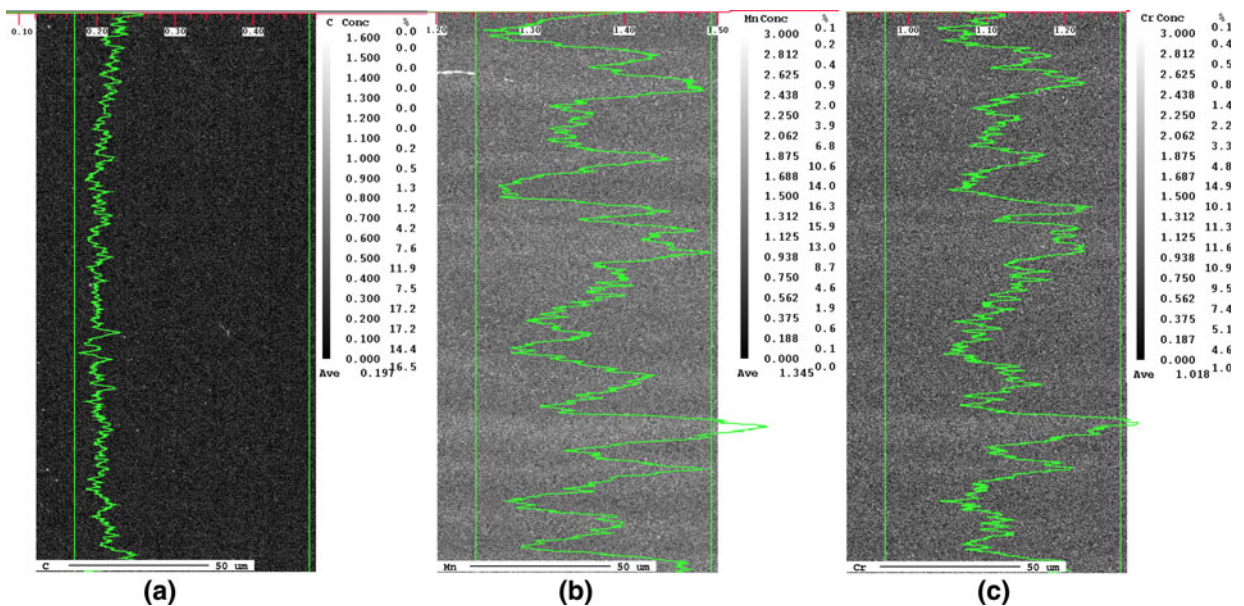


Fig. 5—Electron microprobe analyses of the carbon (a), manganese (b), and chromium (c) concentration in a region of 100 × 200 μm in a sample after heat treatment.

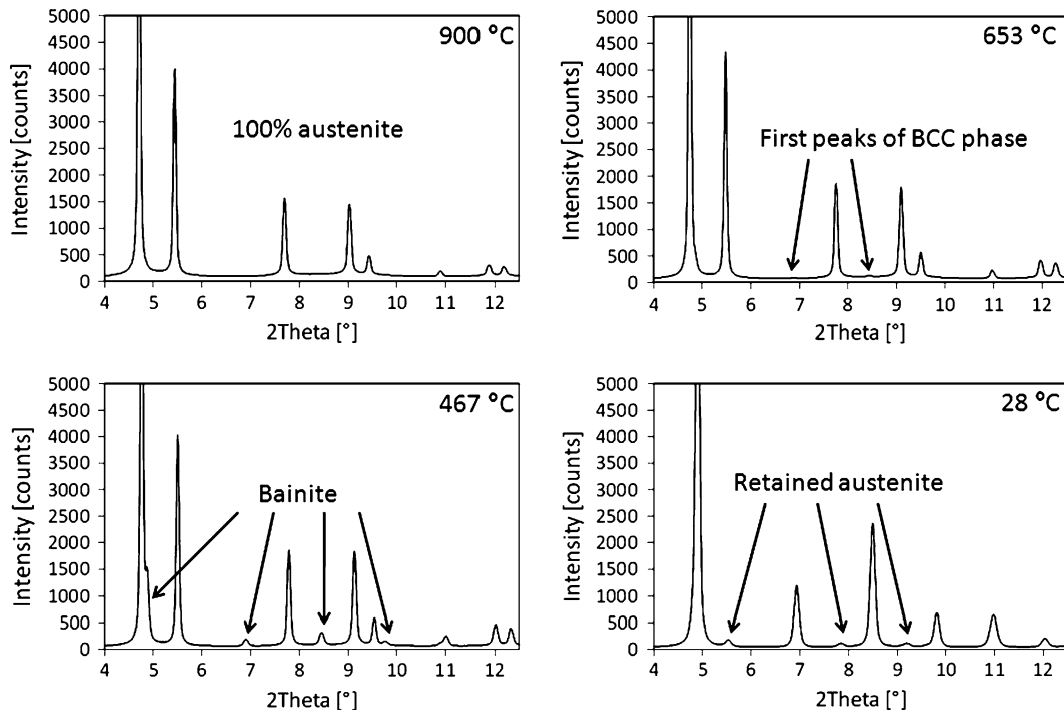


Fig. 7—Diffraction patterns collected at different temperatures during quenching.

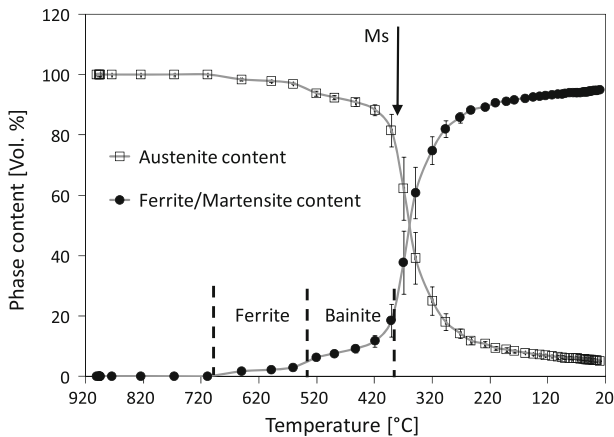


Fig. 8—Evolution of phase fractions during quenching from austenitizing temperature.

diffraction patterns. However, it should be kept in mind that if  $\text{Fe}_3\text{C}$  forms during the bainitic transformation, for an amount of 17 pct of bainite formed from austenite with 0.2 mass pct C, an amount of 0.51 vol pct  $\text{Fe}_3\text{C}$  would be formed. If  $\text{Fe}_{2.4}\text{C}$  forms instead of  $\text{Fe}_3\text{C}$ , the maximum amount of carbide that can be reached is even lower (0.4 vol pct). As a result of the low symmetry of these carbides' crystal structure, it would be very difficult to distinguish any diffraction line for such a small amount. Moreover, already known “carbide-free-bainite” might be formed during cooling accompanied by a carbon partitioning from the BCC phase into the surrounding austenitic matrix.<sup>[22]</sup>

The rate of martensitic transformation is very fast in the first stages of the transformation and becomes more

and more sluggish during cooling. At room temperature, an amount of 4 pct of untransformed austenite remains in the microstructure. For this steel grade, almost no retained austenite was expected as the martensite start temperature is high. However, as shown in Figure 8, austenite seems to be more and more stabilized during cooling.

The processes of carbon redistribution might take place during quenching, particularly if transformation temperatures are high. Moreover, it is well known that increasing carbon content in solution in austenite decreases the martensite start temperature considerably. To check whether a carbon redistribution process is occurring during quenching, inducing a dynamic stabilization of the retained austenite, the evolution of lattice parameters of martensite and austenite was studied in detail and estimations of carbon content in solution were performed.

The carbon content in solution in martensite during cooling can be obtained with Eq. [1].<sup>[23]</sup> For this, the ratio of martensite lattice parameters  $c/a$  is calculated, and from the known linear dependence over carbon content, the carbon content in solution can be obtained at each temperature. The advantage of this method is that errors associated with temperature, thermal expansion correction, or stresses are strongly reduced.

$$\%C_M = \frac{\left(\frac{c_M}{a_M} - 1\right)}{0.0443} \quad [1]$$

The evolution of measured lattice parameters as well as the calculated carbon content from Eq. [1] is presented in Figure 9 as a function of temperature. In



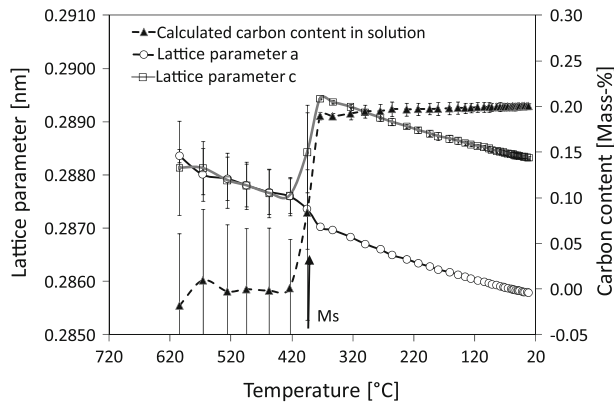


Fig. 9—Evolution of lattice parameters of ferrite/martensite as a function of temperature and calculated carbon content in solution.

the first stages of quenching above  $M_s$ , measured lattice parameters present high standard deviations. However, it can be observed that the lattice parameters “a” and “c” have almost the same value leading to a  $c/a$  ratio close to one and a calculated carbon content around 0 as expected during the creation of ferrite/bainite with a BCC structure.

When the martensite start temperature is reached, lattice parameter “c” increases quickly to reach a maximum value where it then starts to decrease linearly during further cooling. The lattice parameter “a” decreases continuously during the whole quenching process. The resulting carbon content calculated from the  $c/a$  ratio increases quickly to a value of 0.189 mass pct at  $M_s$  and then increases slightly to reach 0.20 mass pct at room temperature. When  $M_s$  is reached, error bars become very small indicating a very good agreement between both experiments.

The same detailed analysis of retained austenite lattice parameters was performed. To determine the evolution of the carbon content in solution, the experimentally determined equation of Onink was used (Eq. [2]).<sup>[24]</sup> In that equation, the effect of the carbon content ( $f_c$  in at. pct) on the thermal expansion coefficient is taken into account. The temperature  $T$  is in Kelvin.

$$a_\gamma(f_c, T) = (0.363067 + 0.000783 \times f_c) \times (1 + (24.92 - 0.51 \times f_c) \times 10^{-6}[T - 1000]) \quad [2]$$

After conversion from at. pct to mass pct, the results were plotted in Figure 10. The straight line represents the theoretical lattice parameter for 0 pct of carbon calculated with Eq. [2]. It can be observed that the curve of measured lattice parameters is roughly parallel to the theoretical line from 1173 K (900 °C) to 793 K (520 °C). The average calculated carbon content in that temperature range is around 0.21 mass pct. This fits to the nominal carbon content of this steel (0.204 mass pct). From 723 K (450 °C) until  $M_s$ , the calculated carbon content increases. During cooling below  $M_s$  (663 K (390 °C)), the measured lattice parameters deviates continuously from the 0 pct C line and consequently

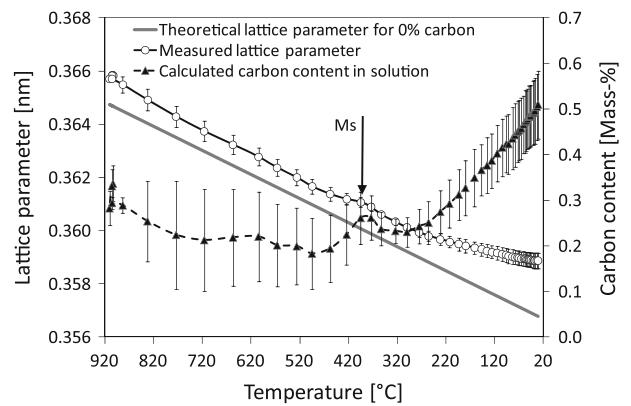


Fig. 10—Evolution of the austenite lattice parameter as a function of temperature and calculated carbon content in solution.

the calculated carbon content increases to reach 0.5 mass pct at room temperature.

Of course, it is not possible to calculate any carbon content from lattice parameter variations without addressing the question of residual stresses created during quenching, and resulting in an additional impact on calculated carbon contents. An “apparent” residual strain at room temperature can be calculated from measured lattice parameters and theoretical lattice parameters for 0.2 mass pct of carbon in retained austenite. If then additionally a hydrostatic stress state is assumed, resulting residual stresses of +1700 MPa in austenite are calculated. This value is unrealistically high. The results of room temperature residual stress measurements of the considered samples with the standard  $\sin^2\psi$  method were  $26 \pm 106$  MPa for the retained austenite and  $276 \pm 16$  MPa for the martensite. The high standard deviation of the retained austenite measurement is from the very low austenite content ( $\approx 4$  mass pct). For these measurements, a possible contribution of residual stresses normal ( $\sigma_{33}$ ) to surface was not considered. However, it is proved from these results that lattice parameter variations are certainly not a result of residual stresses, but mainly they result from carbon partitioning. Moreover, it has already been reported that during standard quenching processes, the martensite phase should be in tension and the small amount of retained austenite should present high stresses of opposite sign to fulfill the force balance.<sup>[23]</sup> This indicates that calculated carbon contents might even underestimate the effect of carbon redistribution.

One remaining question about the origin of carbon redistribution processes is still open. In Figure 8, the determined phase fractions during cooling indicate a small amount of bainite ( $\approx 17$  vol pct) forming above  $M_s$ . Yet, no carbide precipitation could be detected during the formation of bainite, and it is known that the formation of bainite occurring before the martensite transformation may induce a stabilization of the retained austenite.<sup>[25]</sup> The role of bainite formation on the carbon redistribution process is not completely investigated. Additional experiments will be needed to clarify this issue properly.

#### IV. MODELING OF THE TRANSFORMATION KINETIC

Nowadays, most computer simulations are done using the Koistinen-Marburger equation to determine the phase fractions of transformed martensite during cooling.<sup>[26,27]</sup> Equation [3] provides the volume of untransformed austenite as a function of the volume percentage of austenite present just above  $M_s$  ( $A$ ), the temperature  $Tq$  below  $M_s$  and the parameter  $b$ , which is commonly kept constant for most steels at the value of 0.011.<sup>[28]</sup>

$$V_A = A \times \exp[-b(Ms - Tq)] \quad [3]$$

This equation was used with  $M_s = 663$  K (390 °C) to calculate the martensitic transformation kinetics and compare it with the experimental data in Figure 11. The agreement between experimentally determined phase fractions and the results of the Koistinen-Marburger equation are not quite satisfying. In particular, the theoretical results clearly underestimate the retained austenite content reached at room temperature (around 1.5 vol pct), while 4 vol pct was found experimentally. The discrepancies might be attributed to the phenomenon of dynamic austenite stabilization by carbon enrichment as found in these samples.

To model the transformation kinetics more precisely, a slight modification of the Koistinen-Marburger equation can be introduced as proposed by Wildau (Eq. [4]).<sup>[29]</sup>

$$V_A = A \times \exp[-b(Ms - Tq)^n] \quad [4]$$

The two major differences between Eqs. [3] and [4] are that parameter  $b$  is not fixed anymore and an exponent  $n$  is added. According to the first study with this equation, parameters  $b$  and  $n$  depend on the martensite start temperature.<sup>[26]</sup> To model the transformation kinetics with Eq. [4], parameters  $b$  and  $n$  were fitted to experimental values by the least-squares method. The values of both parameters after refinement are  $b = 0.0662$  and  $n = 0.663$ .

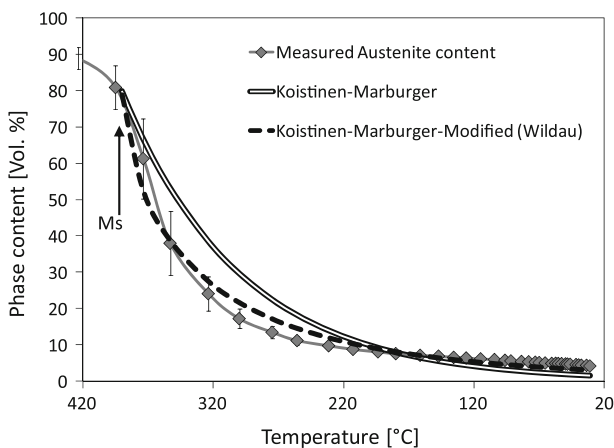


Fig. 11—Experimentally determined martensite transformation kinetic as well as modeled kinetic by the Koistinen-Marburger equation and by a modification of this equation.

The modeled kinetic is also presented in Figure 11. It can be observed that the agreement between experimental values and model is still not perfect, but it is much better than what is obtained by the original Koistinen-Marburger equation (Eq. [4]). In particular, it can be observed that the predicted amount of retained austenite at room temperature is much closer to the experimental value. A quantitative comparison of the agreement between both models and the experimental data is given by the coefficients of determination obtained for both regressions:  $R^2 = 0.938$  for the Koistinen-Marburger equation (Eq. [4]) and  $R^2 = 0.982$  for the modified equation of Wildau (Eq. [4]).

According to these results, the Koistinen-Marburger equation cannot be used to predict reliable martensite transformation kinetics in low carbon steel where dynamic austenite stabilization from carbon redistribution processes occur. The use of the modified Koistinen-Marburger equation with the parameters  $b$  and  $n$  adapted to the steel grade and the cooling conditions seem to be more indicated.

#### V. CONCLUSIONS

With the high intensity and energy of synchrotron radiation, phase transformation kinetics during rapid cooling of a typical carburizing steel grade could be investigated in detail. Precise phase content evolutions could be obtained by means of Rietveld refinements of measured diffraction patterns. Transformation of a small amount of bainite could be observed before the martensitic transformation starts at 663 K (390 °C). The amount of retained austenite determined at room temperature was unexpectedly high for this steel grade.

Detailed analysis of lattice parameter evolution of martensite and austenite during quenching allowed identifying a carbon redistribution process. This results in a carbon enriched austenite (approximately 0.5 mass pct C). The carbon enrichment of austenite explains the high amount of retained austenite at room temperature as a result of a dynamic stabilization. However, the origin of the carbon enrichment is not completely clear and will be further investigated. In particular, experiments with higher cooling rate implying no bainite formation will be performed.

The modeling of transformation kinetics could not be achieved properly with the original Koistinen-Marburger equation, probably as a result of the dynamic stabilization of retained austenite. A modified equation proposed by Wildau with two refinable parameters allowed for modeling the martensitic phase transformation to fit experimental data. The use of this model with parameters adapted to the considered steel grade and cooling condition is recommended.

#### ACKNOWLEDGMENTS

The authors gratefully acknowledge the Deutsche Forschungsgemeinschaft (DFG) for financial support

of project C2 in the Collaborative Research Centre 570 “Distortion Engineering” and the European Synchrotron Radiation Facility (ESRF) for provision of synchrotron radiation facilities.

## REFERENCES

1. G.B. Olson and W.S. Owen: *Martensite*, 1st ed., ASM International, Materials Park, OH, 1992.
2. S.G. Fletcher: *The Tempering of Plain Carbon Steels*, Carnegie Institute of Technology, Pittsburgh, PA, 1938.
3. Z. Nishiyama, M.E. Fine, M. Meshii, and C.M. Wayman: *Martensitic Transformation*, Academic Press, New York, NY, 1978.
4. G.V. Kurdjumov and A.G. Khachaturyan: *Acta Metall.*, 1975, vol. 23, pp. 1077–88.
5. G.V. Kurdjumov: *Metall. Trans. A*, vol. 7A, 1976, pp. 999–1011.
6. Metals Handbook: *Properties and Selection: Irons, Steels, and High-Performance Alloys*, 10th ed., vol. 1, ASM International, Materials Park, OH, 1990.
7. F. Frerichs, T. Lübben, U. Fritsching, H. Lohner, A. Rocha, G. Löwisch, F. Hoffmann, and P. Mayr: *J. Phys. IV*, 2004, vol. 120, pp. 727–35.
8. C. Acht, B. Clausen, F. Hoffmann, and H.W. Zoch: *Proc. 1st Int. Conf. on Distortion Engineering*, H.W. Zoch and T. Lübben, eds., Bremen, Germany, 2005, pp. 251–58.
9. F. Frerichs, T. Lübben, F. Hoffmann, and H.-W. Zoch: *Num. Steel Res. Int.*, 2007, vol. 78 (7), pp. 558–63.
10. D.H. Sherman, S.M. Cross, S. Kim, F. Grandjean, G.J. Long, and M.K. Miller: *Metall. Mater. Trans. A*, 2007, vol. 38A, pp. 1698–711.
11. M. Sariyaka, G. Thomas, J.W. Steeds, S.J. Barnard, and G.D.W. Smith: *International Conference on Solid to Solid Phase Transformations*, H.I. Aaronson, ed., TMS, Warrendale, PA, 1982, pp. 1421–25.
12. S. Chupatanakul, P. Nash, and D. Chen: *Metall. Mater. Int.*, 2006, vol. 12 (6), pp. 453–58.
13. A.J. Clarke, J.G. Speer, M.K. Miller, R.E. Hackenberg, D.V. Edmonds, D.K. Matlock, F.C. Rizzo, K.D. Clarke, and E. De Moor: *Acta Mater.*, 2008, vol. 56, pp. 16–22.
14. D.V. Edmonds, K. He, F.C. Rizzo, B.C. De Cooman, D.K. Matlock, and J.G. Speer: *Mater. Sci. Eng. A*, 2006, vols. 438–40, pp. 25–34.
15. J. Epp, H. Surm, O. Kessler, and T. Hirsch: *Metall. Mater. Trans. A*, 2007, vol. 38A, pp. 2371–78.
16. J. Epp, H. Surm, O. Kessler, and T. Hirsch: *Acta Mater.*, 2007, pp. 5517, 5959–67.
17. J.-C. Labiche, O. Mathon, S. Pascarelli, M.A. Newton, G.G. Ferre, C. Curfs, G. Vaughan, and A. Homs: *Review Sci. Instr.*, 2007, vol. 78, pp. 1–11.
18. A. Hammersley, S.O. Svensson, and A. Thompson: *Nucl. Instrum. Methods*, 1994, vol. A (346), p. 312.
19. B.E. Warren: *X-Ray Diffraction*, Addison-Wesley, Reading, MA, 1969.
20. E.C. Bain: *The Alloying Elements in Steel*, ASM International, Materials Park, OH, 1939.
21. Doerrenberg Edelstahl – Datasheet 21MnCr5, [http://www.doerrenberg.de/fileadmin/template/doerrenberg/stahl/DatenblaetterEng/1.2162\\_en.pdf](http://www.doerrenberg.de/fileadmin/template/doerrenberg/stahl/DatenblaetterEng/1.2162_en.pdf), 08.30.2011.
22. S. Khare, K. Lee, and H.K.D.H. Bhadeshia: *Metall. Mater. Trans. A*, 2010, vol. 41A, pp. 922–28.
23. L. Cheng, A. Böttger, T.H. de Keijser, and E.J. Mittemeijer: *Scripta Metall. Mater.*, 1990, vol. 24, pp. 509–14.
24. M. Onink, C.M. Brakman, F.D. Tichelaar, E.J. Mittemeijer, and S. van der Zwaaag: *Acta Metall. Mater.*, 1993, vol. 29, pp. 1011–16.
25. G.B. Olson, H.K.D.H. Bhadeshia, and M. Cohen: *Acta Metall.*, 1989, vol. 2 (37), pp. 381–89.
26. S.-H. Kanga and Y.-T. Imb: *J. Mater. Proc. Tech.*, 2007, vol. 183, pp. 241–44.
27. J.W. Janga, I.-W. Parkb, K.H. Kimb, and S.S. Kanga: *J. Mater. Proc. Tech.*, 2002, vols. 130–131, pp. 546–50.
28. D.P. Koistinen and R.E. Marburger: *Acta Metall.*, 1959, vol. 7, pp. 59–60.
29. M. Wildau: Ph.D. Dissertation, Technical University of Aachen, Aachen, Germany, 1986.